Electronic Supplementary Information

Controllable Fabrication of Bio-bar Codes for Dendritically Amplified Sensing of Human T-lymphotropic Viruses

Li-juan Wang, [#,†] Ming Ren, [#,†] Li Liang, [‡,†] and Chun-yang Zhang[#,*]

[#] College of Chemistry, Chemical Engineering and Materials Science, Collaborative Innovation Center of Functionalized Probes for Chemical Imaging in Universities of Shandong, Key Laboratory of Molecular and Nano Probes, Ministry of Education, Shandong Provincial Key Laboratory of Clean Production of Fine Chemicals, Shandong Normal University, Jinan 250014, China.

[‡] Department of Tumor Chemotherapy and Radiation Sickness, Peking University Third Hospital, Beijing 100191, China

* Corresponding author. Tel.: +86 0531-86186033; Fax: +86 0531-82615258. E-mail: cyzhang@sdnu.edu.cn.

1. Optimization of Experimental Conditions

To achieve the best performance, we optimized the experimental conditions including the polymerization time of the TdT-catalyzed two-step extension reactions, the concentrations of hemin, luminol and HEPES, and the ratio of dATP to dGTP. The polymerization time influences the length of extension products and eventually the dendritic amplification efficiency of bio-bar codes. In the TdT-catalyzed first-step polymerization reaction, the size of poly-T DNA band enlarges with the reaction time from 5 to 120 min (Fig. S1A, lanes 2-6), indicating that the long polymerization time induces the incorporation of more dTTPs into the 3′-OH end of HTLV-II DNA for the generation of a longer poly-T sequence. In addition, we measured the variance of chemiluminescence intensity with the reaction time of TdT-catalyzed first-step polymerization extension. As shown in Fig. S1B, the chemiluminescence intensity enhances rapidly from 5 to 30 min and reaches a plateau at 30 min, indicating that 30 min is the optimal reaction time for TdT-catalyzed first-step polymerization extension. We further optimized the reaction time of the TdT-catalyzed second-step polymerization extension. As shown in Fig. S1C, the size of G-rich DNA bands enlarges as a function of reaction time from 5 to 60 min (Fig. S1C, lanes 2-6). Interestingly, the chemiluminescence intensity enhances with the reaction time and reaches the highest value at 20 min (Fig. S1D). The discrepancy between Fig. S1C and Fig. S1D may be explained by that the generation of an extremely long G-rich DNA product after 20 min (Fig. S1C) may pose a steric hindrance for the formation of functional G-quadruplex structures which are proportional to the chemiluminescence intensity (Fig. S1D). Thus, 20 min is selected as the optimal reaction time of TdT-catalyzed second-step polymerization extension. Notably, under the same reaction time, the length of poly-T products obtained in the first-step polymerization reaction (Fig. S1A) is much longer than that of G-rich products obtained in the

second-step polymerization reaction (Fig. S1C), suggesting that TdT can incorporate more mononucleotides into the 3′-OH end of ssDNA fragments in the presence of a dTTP pool than in the presence of a dNTP pool (60% dGTPs and 40% dATPs).[1-4] In addition, we optimized the hemin concentration. Due to the dependence of catalytic kinetic of luminol-H_2O_2 reaction upon the hemin concentration,[5] the chemiluminescence intensity enhances with the increasing concentration of hemin no matter the G-rich polymerization products are present or not.[6] As shown in Fig. S1E, the I/I_0 value enhances with the increasing concentration of hemin from 0.75 to 750 nM, followed by a sharp decrease beyond the concentration of 750 nM due to the relatively high background signal (i.e. I_0) induced by high-concentration hemin (I and I_0 are the chemiluminescence intensity in the presence and absence of the G-rich polymerization products, respectively). Thus, 750 nM hemin is used in the subsequent research. We further optimized the luminol concentration. As shown in Fig. S1F, the I/I_0 value improves with the increasing concentration of luminol from 0.05 to 0.5 mM, followed by the decrease beyond the concentration of 0.5 mM due to the relatively high background signals (i.e. I_0) induced by high-concentration luminol. Thus, 0.5 mM luminol is used in the subsequent research. Taking into account the effect of pH value upon the H_2O_2-catalyzed luminol oxidation reaction, we optimized the HEPES concentration. As shown in Fig. S1G, the I/I_0 value enhances with the increase of HEPES concentration from 10 to 40 mM and reaches the highest value at the concentration of 40 mM, followed by decrease beyond the concentration of 40 mM due to the inhibition of luminol-H_2O_2 reaction by high-concentration HEPES which leads to low pH value. Thus, 40 mM is selected as the optimal HEPES concentration in subsequent research. We further optimized the dATP-to-dGTP ratio to obtain the efficient G-rich DNAzyme. As shown in Fig. S1H, the chemiluminescence intensity increases with the decrease of dATP-to-dGTP ratio from 100%:0%

to 40%:60% and reaches the maximum value at the ratio of 40%:60%, followed by the decrease beyound the radio of 40%:60%. Thus, 40%:60% is selected to be the optimal dATP-to-dGTP ratio in subsequent research.

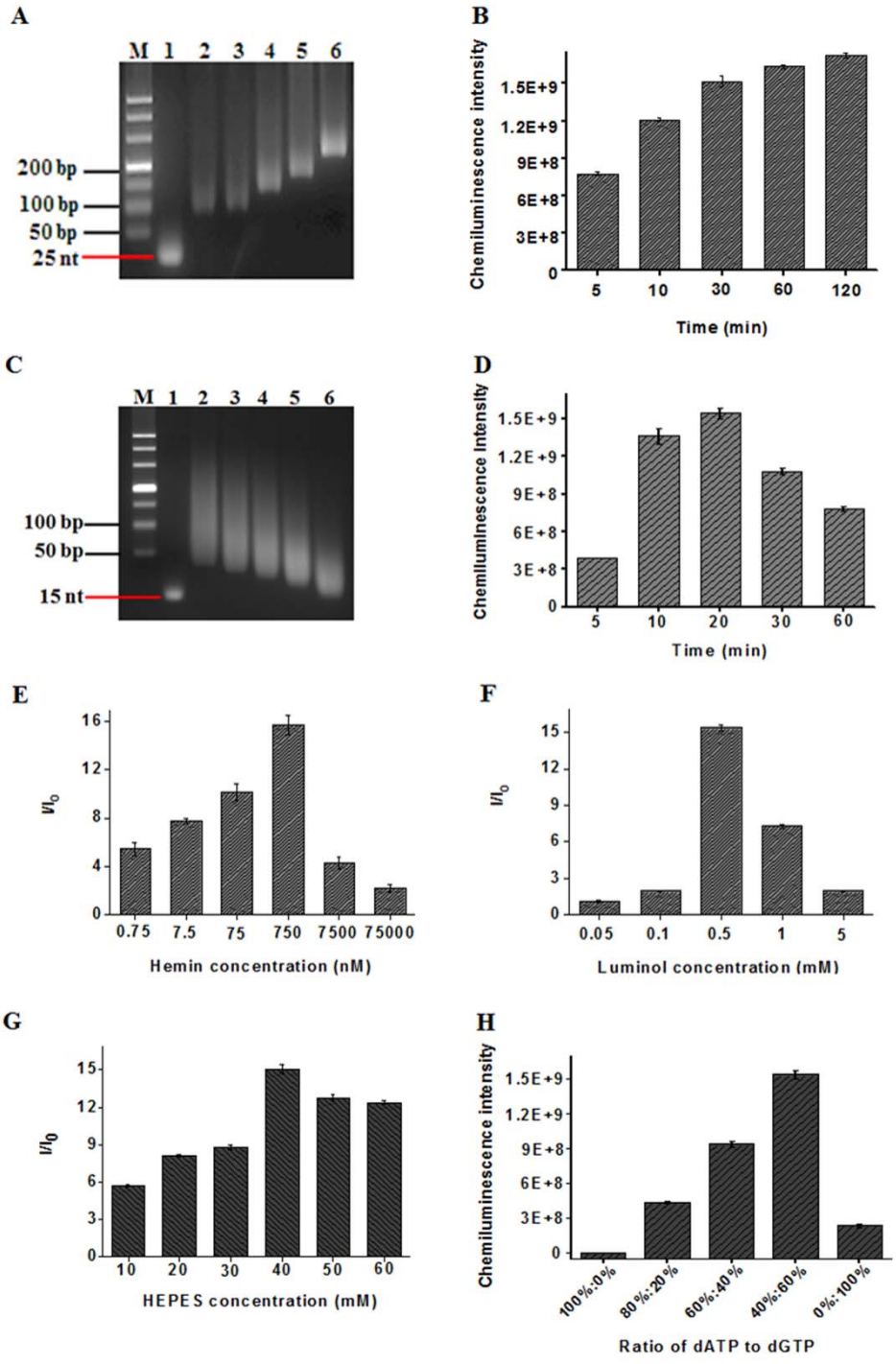

Fig. S1 (A) Agarose gel electrophoresis analysis of TdT-catalyzed first-step polymerization products at different reaction time in the presence of 0.4 U TdT and 10 μM dTTPs. Lane M is the DNA

marker; Lane 1 shows the products in the absence of TdT; Lanes 2-6 show the products in the presence of TdT at reaction time of 5, 10, 30, 60, and 120 min, respectively. (B) Variance of chemiluminescence intensity with reaction times in A. (C) Agarose gel electrophoresis analysis of TdT-catalyzed second-step polymerization products at different reaction time in the presence of 0.4 U TdT and 10 μM dNTPs. Lane M is the DNA marker; Lane 1 shows the products in the absence of TdT; Lanes 2-6 show the products in the presence of TdT at reaction time of 60, 30, 20, 10, and 5 min, respectively. (D) Variance of chemiluminescence intensity with reaction times in C. (E) Variance of the I/I_0 value as a function of hemin concentration. I and I_0 are the chemiluminescence intensity in the presence and absence of the G-rich polymerization products, respectively. (F) Variance of the I/I_0 value as a function of luminol concentration. I and I_0 are the chemiluminescence intensity in the presence and absence of the G-rich polymerization products, respectively. (G) Variance of the I/I_0 value as a function of HEPES concentration. I and I_0 are the chemiluminescence intensity in the presence and absence of the G-rich polymerization products, respectively. (H) Variance of chemiluminescence intensity in response to different ratio of dATP to dGTP. In E, F, G and H, the amount of TdT in the first-step polymerization reactions is 0.4 U, and the amount of TdT in the second-step polymerization reactions is 0.4 U. Error bars show the standard deviations of three experiments.

2. Monitoring of chemiluminescence intensity in the presence and absence of capture probe 2-/reporter probe-functionalized AuNPs

To investigate the improved sensitivity, we measured the chemiluminescence intensity with/without the involvement of capture probe 2-/reporter probe-functionalized AuNPs, respectively. When

HTLV-II DNA is present, it hybridizes with the MMP-modified capture probe 1 to form a stable double-stranded DNA (dsDNA) duplex with a protruding 3'-hydroxylated sequence. Upon the addition of TdT and a dNTP pool (60% dGTPs and 40% dATPs), the chemiluminescence intensity is measured. As shown in Fig. S2, in the presence of 1 nM HTLV-II DNA, a low chemiluminescence signal is detected (Fig. S2, blue column) without the involvement of capture probe 2-/reporter probe-functionalized AuNPs. While with the addition of capture probe 2-/reporter probe-functionalized AuNPs, HTLV-II DNA initiates the TdT-catalyzed first-step enzymatic extension to produce the poly-T sequence for dendritic self-assembly of capture probe 2-/reporter probe-functionalized AuNPs, subsequently triggering the second-step enzymatic extension to produce the G-rich DNAzyme for the generation of chemiluminescence signal. Consequently, the addition of capture probe 2-/reporter probe-functionalized AuNPs induces 913.30-fold chemiluminescence enhancement (Fig. S2, red column) as compared with that without the involvement of capture probe 2-/reporter probe-functionalized AuNPs (Fig. S2, blue column).

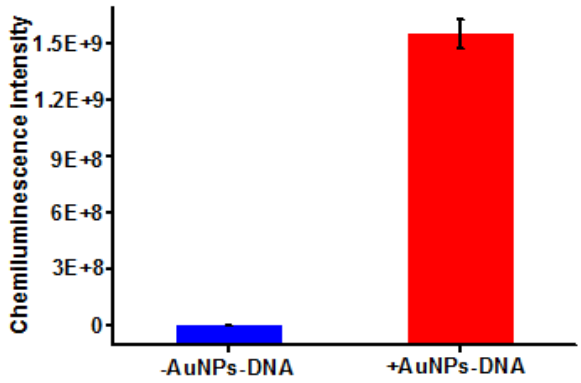

Fig. S2 Measurement of chemiluminescence intensity without (blue column) and with the involvement of capture probe 2-/reporter probe-functionalized AuNPs (red column), respectively. The concentration of HTLV-II DNA is 1 nM. Error bars show the standard deviations of three experiments.

3. Detection of HTLV-II DNA by real-time quantitative PCR (qPCR)

To quantify the amount of HTLV-II DNA in genomic DNA samples (Fig. 5B), we performed quantitative real-time fluorescence measurement in response to different concentrations of synthesized HTLV-II DNA using SYBR Green I as the fluorescent indicator. As shown in Fig. S3A, HTLV-II DNA is detected quantitatively in the range from 10^{-14} M to 10^{-11} M. The real-time fluorescence intensity increases in a sigmoidal fashion as HTLV-II DNA is converted from a single-stranded to a partially double-stranded DNA duplex. The threshold cycle (C_T) indicates the fractional cycle number at which amount of amplified target reaches a fixed threshold,[7] which is used for the quantitative detection of the starting quantity of HTLV-II DNA. As shown in Fig. S3B, a linear correlation is obtained between the C_T values and the logarithmic starting quantity of HTLV-II DNA in the range from 10^{-14} to 10^{-11} M. The correlation equation is $C_T = -9.92 - 2.56 \log_{10} C$ with a correlation coefficient of 0.9959, where C is the starting quantity of HTLV-II DNA.

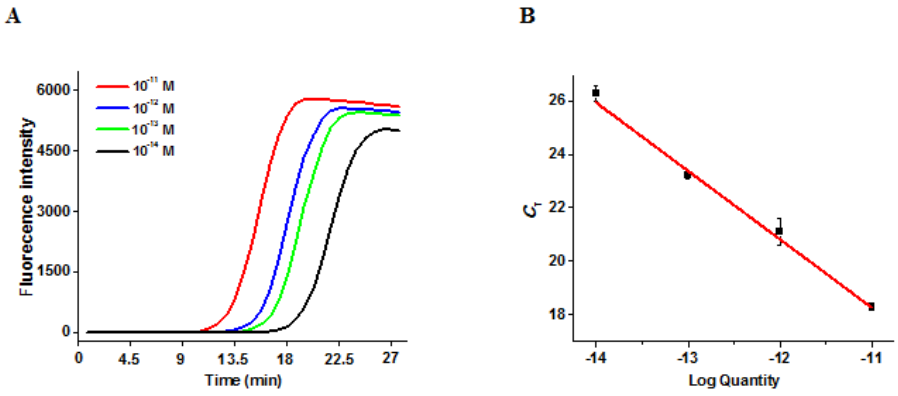

Fig. S3 (A) Quantitative real-time fluorescence monitoring of the PCR amplification reaction triggered by different starting quantity of HTLV-II DNA. (B) Variance of the C_T value as a function of the logarithmic starting quantity of HTLV-II DNA. Error bars show the standard deviations of three experiments.

Table S1. **Comparison of our method with the reported methods for nucleic acid assay**

method	use of nanomaterial	LOD[a]	order of dynamic range	target	real sample analysis	ref.
BCA[b]-based fluorescent assay	yes	2.5 fM	3 (2.5 fM-1 pM)	DNA	bacterial genomic DNA	8
PCR[c]-based fluorescent assay	no	5 fM	4 (500 fM-5 nM)	DNA	cell lysate	9
RCA[d]-based fluorescent assay	no	12 aM	1 (15 aM-0.9 fM)	miRNA	cell extracts	10
HCR[e]-based electrochemical assay	no	9 fM	3 (0.1 pM-250 pM)	DNA	no	11
CHA[f]-based electrochemical assay	no	92 fM	4 (0.1 pM-5 fM)	DNA	cell lysate and serum	12
LCR[g]-based gel analysis	no	2 pM	3 (2 pM-2 nM)	miRNA	no	13
endonuclease-assisted fluorescent assay	yes	198 fM	1 (1 pM-50 pM)	DNA	serum	14
exonuclease-assisted electrochemical assay	no	20 pM	1 (20 pM-300 pM)	DNA	no	15
endonuclease-assisted colorimetric assay	yes	1 pM	0	DNA	cell extracts	16
cascade enzymatic cleavage-based electrochemical assay	no	10 fM	2 (1 pM-100 pM)	DNA	no	17
DNAzyme-mediated electrochemical assay	no	0.03 fM	6 (0.1 fM-0.1 nM)	DNA	no	18
hairpin probe assisted-colorimetric assay	yes	100 aM	7 (10 fM-100 nM)	DNA	no	19
enzymatic amplification -	no	33 pM	5	HTLV-	no	20

mediated electrochemical assay			(0.1 fM-1 nM)	II DNA		
bio-bar-code-based chemiluminescent assay	yes	0.5 aM	9 (1 aM-1 nM)	HTLV-II DNA	cell extracts and serum	this work

[a] LOD, limit of detection, [b] BCA, bio-bar-code amplification, [c] PCR, polymerase chain reaction, [d]RCA, rolling circle amplification, [e] HCR, hybridization chain reaction, [f] CHA, catalyzed hairpin assembly, [g] LCR, ligase chain reaction.

References

1. C.-P. D.; Cohen, S. N. *Gene* **1980**, *10*, 177-183.
2. Boulé, J.-B.; Rougeon, F.; Papanicolaou, C. *J. Biol. Chem.* **2001**, *276*, 31388-31393.
3. Chang, L. M. S.; Bollum, F. J.; Gallo, R. C. *Crit. Rev. Biochem.* **1986**, *21*, 27-52.
4. Roychoudhury, R.; Jay, E.; Wu, R. *Nucleic Acids Res.* **1976**, *3*, 863-878.
5. Travascio, P.; Bennet, A. J.; Wang, D. Y.; Sen, D. *Chem. Biol.* **1999**, *6*, 779-787.
6. Wang, L.-j.; Zhang, Y.; Zhang, C.-y. *Anal. Chem.* **2013**, *85*, 11509-11517.
7. Livak, K. J.; Schmittgen, T. D. *Methods* **2001**, *25*, 402-408.
8. Hill, H. D.; Vega, R. A.; Mirkin, C. A. *Anal. Chem.* **2007**, *79*, 9218-9223.
9. Yu, C.-Y.; Yin, B.-C.; Wang, S.; Xu, Z.; Ye, B.-C. *Anal. Chem.* **2014**, *86*, 7214-7218.
10. Liu, H.; Li, L.; Duan, L.; Wang, X.; Xie, Y.; Tong, L.; Wang, Q.; Tang, B. *Anal. Chem.* **2013**, *85*, 7941-7947.
11. Li, C.; Wang, H.; Shen, J.; Tang, B. *Anal. Chem.* **2015**, *87*, 4283-4291.
12. Tao, C.; Yan, Y.; Xiang, H.; Zhu, D.; Cheng, W.; Ju, H.; Ding, S. *Chem. Commun.* **2015**, *51*, 4220-4222.

13. Yan, J.; Li, Z.; Liu, C.; Cheng, Y. *Chem. Commun.* **2010**, *46*, 2432-2434.

14. Li, N.; Gao, Z. F.; Kang, B. H.; Li, N. B.; Luo, H. Q. *RSC Adv.* **2015**, *5*, 20020-20024.

15. Xuan, F.; Luo, X.; Hsing, I. M. *Anal. Chem.* **2012**, *84*, 5216-5220.

16. Zou, B.; Cao, X.; Wu, H.; Song, Q.; Wang, J.; Kajiyama, T.; Kambara, H.; Zhou, G. *Biosens. Bioelectron.* **2015**, *66*, 50-54.

17. Liu, S.; Liu, T.; Wang, L. *Chem. Commun.* **2015**, *51*, 176-179.

18. Yuan, L.; Tu, W.; Bao, J.; Dai, Z. *Anal. Chem.* **2015**, *87*, 686-692.

19. Liu, J.; Chen, L.; Lie, P.; Dun, B.; Zeng, L. *Chem. Commun.* **2013**, *49*, 5165-5167.

20. Shen, Q.; Han, L.; Fan, G.; Zhang, J.-R.; Jiang, L.; Zhu, J.-J. *Anal. Chem.* **2015**, *87*, 4949-4956.